Acta Odontologica Scandinavica. 2015; 73: 302–311

informa
healthcare

ORIGINAL ARTICLE

Ultraviolet-C irradiation to titanium implants increases peri-implant bone formation without impeding mineralization in a rabbit femur model

MAKOTO YAMAZAKI[1], MASAHIRO YAMADA[1,2], KEN ISHIZAKI[1] & KAORU SAKURAI[1]

[1]*Department of Removable Prosthodontics and Gerodontology, and* [2]*Oral Health Science Center, Tokyo Dental College, Tokyo, Japan*

Abstract

Objectives. Volume and bone quality of peri-implant supporting bone, in particular, at implant neck region, as well as bone–implant contact ratio, is important for long-term stability of implants. Ultraviolet-C (UVC) irradiation is known to enhance the osseointegration capability of titanium implants. However, the histological determination was performed only on a rat model, but not pre-clinical animal model such as a rabbit model. The purpose of this study was to determine the effects of UVC irradiation on titanium implants on the volume and mineral density of peri-implant supporting bone formation in a rabbit femur model. ***Materials and methods.*** Acid-etched pure titanium screw implants with or without 3 mW/cm^2 UVC irradiation for 48 h were placed in rabbit femur diaphyses. Peri-implant bone tissue formation was analyzed at 3 and 8 weeks post-operatively by histology and micro-CT-based bone morphometry after calibration with hydroxyl apatite phantoms. ***Results.*** UVC pre-irradiated implants accumulated a higher density of cells and thicker and longer bone tissue attachments that continued into the inner basic lamellae of the surface of existing cortical bone at 3 and 8 weeks than the implants without irradiation. Although the bone mineral density around both implants was equivalent to that of the existing cortical bone, bone volume was greater with UVC pre-irradiation in two-thirds or more of the apical region throughout the observation period. ***Conclusions.*** These results indicate that UVC treatment increased the volume of cortical-like bone tissue in the coronal region of titanium implants without deterioration of bone mineral density.

Key Words: *contact osteogenesis, microCT, photo-functionalization, osseointegration, surface modification*

Introduction

Peri-implant tissue consists of an amorphous layer, 50–500 nm in width, at the bone–implant interface and the surrounding, supporting bone tissue [1,2]. Functional loads borne by the implant are transferred to the surrounding, supporting bone tissue through the bone–implant interface. Many studies using finite element analysis have demonstrated that stress points resulting from load on the implant thread that is integrated with bone tissue concentrate peri-implant tissue at the implant neck region [3,4]. The distribution of functional force is mostly concentrated at and beneath the implant neck region in the crestal ridge because implants lack the micro-movements that occur with natural teeth [5]. The application of lateral force increases the tendency for force concentrations at the implant neck region [5]. Concentration of over-stress causes peri-implant bone resorption and eventually leads to implant failure. Peri-implant bone resorption at the implant neck region risks further increasing stress concentrations and subsequent bone resorption in that region [6,7]. In contrast, increases in the volume of supporting bone tissue or bone–implant contact ratio can reduce and de-concentrate the stress distribution in peri-implant bone tissue [8]. Therefore, enhancement of the mechanical strength of the bone–implant interface and the peri-implant supporting bone tissue, in particular at the implant neck region, might alleviate stress concentrations in the tissue, eventually improving the long-term stability of the implant.

Recently, ultraviolet-C (UVC)-mediated functionalization of titanium implant surfaces has been

Correspondence: Masahiro Yamada, DDS PhD, Department of Removable Prosthodontics & Gerodontology, Tokyo Dental College, 2-9-18 Misaki-chou, Chiyoda-ku, Tokyo, 101-0061, Japan. Tel: +81 (0)3 6380 9201. Fax: +81 (0)43 270 3935. E-mail: masayamada@tdc.ac.jp

(Received 18 March 2014; accepted 7 August 2014)

ISSN 0001-6357 print/ISSN 1502-3850 online
DOI: 10.3109/00016357.2014.956332

introduced in numerous articles as a photo-induced surface modification technology that enhances the osseointegration capability of titanium implants. Acid-etched titanium cylinder implants with UVC pre-irradiation at a specific intensity and duration yielded a 98.2% bone–implant contact ratio at 4 weeks after implantation in a rat femur model, in contrast with an ~50% ratio in non-irradiated implants [9]. The osseointegration strength, assessed by delamination forces applied at the bone–implant interface at 4 weeks after implantation was 3.0-times greater for UVC pre-irradiated cylinder-type titanium implants than for non-irradiated implants in a push-in model on the rat femur [9]. After implantation, many original bone fragments remain covering the surface of UVC pre-irradiated implants after being pushed-in, whereas few fragments remain for the most part with non-irradiated implants [10,11].

However, these histological and biomechanical analyses were performed in a rat model using cylindrical mini-implants, but not pre-clinical animal models such as rabbit, dog and sheep, using an actual-size implant. There are considerable dissimilarities between rat and human bone tissue in regard to speed of bone healing or available implant size [12]. In addition, there is little information about the effects of UVC irradiation on peri-implant supporting bone tissue and bone strength-related structural factors, such as bone volume (BV) and bone mineral density (BMD). The quantification of volume and quality of bone tissue is one of traditional methods to evaluate strength of bone tissue. BV, BMD and bone quality measures, such as trabecular number, thickness and separation, are universally used as parameters to evaluate bone structure [13–16]. It is well-known that bone tissue attached on implant surface shows cortical-like, but not trabecular-like, structure [17]. Therefore, quantification of BV and BMD are primary end-points for the evaluation of bone structure formed on implant surfaces. The purpose of this *in vivo* study was to evaluate the effects of UVC pre-irradiation of titanium implants on bone formation in association with BV and BMD, in particular at the implant neck region in a rabbit femur model using micro-computed tomography (micro-CT) analysis and histological observation.

Materials and methods

Titanium implants and surface characterization

Pure titanium (Grade 2) screw-shaped implants with a 0.6 mm thread pitch, 0.3 mm thread depth, 3.75 mm diameter and 6.5 mm length were manufactured by turning machine for this study (Figure 1A). The surface of the implants was prepared by acid-etching with 67% (w/w) sulfuric acid (H_2SO_4) at 120°C for 75 s without pre-processing. Prepared titanium implants were stored under dark ambient conditions for 4 weeks. After storage, 10 titanium implants were irradiated with UVC for 48 h under ambient conditions using a 15 W bactericidal lamp (UV Bench

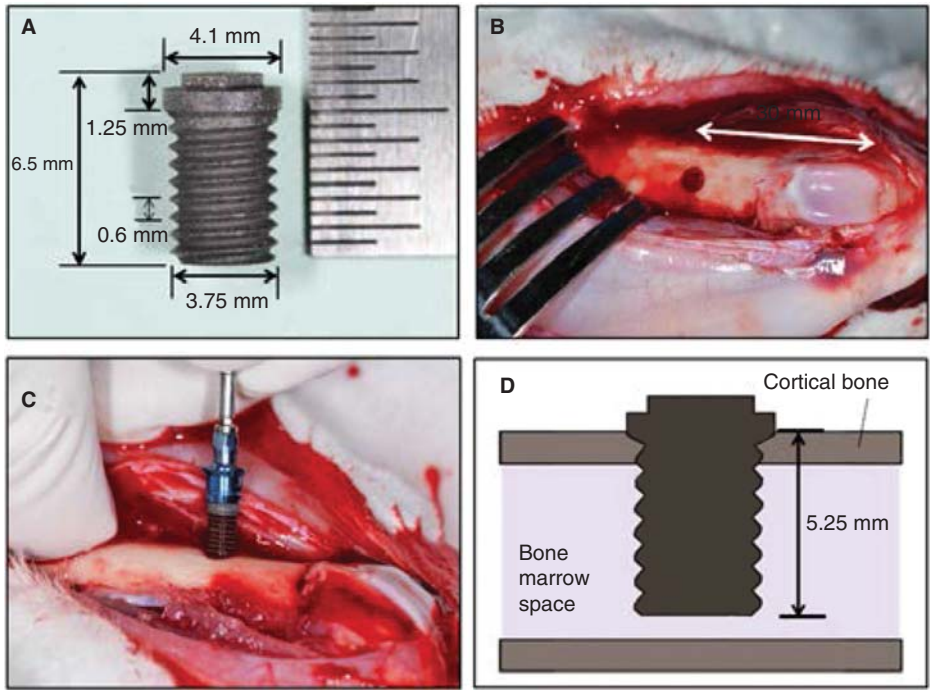

Figure 1. (A) Photograph of an acid-etched titanium implant (6.5 mm length, 3.75 mm diameter) used in this experiment. (B) Top view of a rabbit femur after preparation of the implant hole located at 30 mm from the distal edge of the femur. (C) Side view of a UVC pre-irradiated titanium implant being placed in the implantation hole in a rabbit femur. Note blood climbing up the implant from the bone marrow due to the superhydrophilicity of the implant surface. (D) Schematic diagram of the implant placement in a rabbit femur.

Lamp, 15 W, XX-15S, 254 nm, 100 V, Funakoshi Corporation, Tokyo, Japan) at an intensity of ~3 mW/cm^2. The total energy irradiated on the titanium surfaces was ~518 J/cm^2.

The effects of the UVC treatments on the properties of the titanium surfaces was characterized by determining change of the following three distinct parameters; (1) wettability, (2) chemical composition and (3) surface roughness. The wettability of implant surface with or without UVC treatment was measured as the contact angle of a 10 μL deionized distilled water droplet placed on the apical flat surface of implant using an image analyzer (ImageJ, NIH, Bethesda, ML). The degree of water tensile in contact of the apical top of implant with surface of deionized distilled water was also observed for evaluation of wettability. The chemical composition of the implant surfaces with or without UVC treatment was evaluated by X-ray photoelectron spectroscopy (XPS; AXIS-ULTRA DLD, Shimadzu Corporation, Kyoto, Japan). Surface roughness was evaluated by observation of three-dimensional surface geometry and measurement of surface roughness parameter including arithmetic mean estimation (Ra) and the maximum peak-to-valley roughness height (Ry) using a 3D measuring laser microscope (LEXT OLS4000, Olympus, Tokyo, Japan). Five different spots were measured and the mean value was set as a representative value in each implant. Measurements of wettability and surface roughness were performed on five independent implants.

Animal surgery

Sixteen-week-old male Japanese white rabbits weighing 3.0–3.5 kg were used in this study. Rabbits were anesthetized by intramuscular administration of 2.5% thiopental sodium (Ravonal, Mitsubishi Tanabe Pharma Corporation, Osaka, Japan) before the operation. The thighs were shaved and locally-anesthetized with an injection of 2% lidocaine with 1:80 000 adrenaline (Xylocaine, Dentsply Sankin, Tokyo, Japan). The femurs were exposed by careful elevation of the periosteum after the skin incision and muscle dissection. The flat surfaces of the distal femurs 30 mm from the distal edge of the femur were selected for implant placement (Figure 1B). The 3.6 mm final diameter implantation hole was created using an implant drill under external irrigation with sterile saline. One non-irradiated implant and one UVC pre-irradiated implant were randomly placed into each side of the femur. All implants were placed in such a way that the implant body, from the shoulder down, was located beneath the surface of the femur and a 5.25 mm portion of the implant body from the apex to the shoulder faced the cortical bone and bone marrow tissue (Figures 1C and D). After implantation, the periosteum, muscle and skin were sutured with 3-0 polyglactin suture (Vicryl, Ethicon Japan, Tokyo, Japan). Animals were kept in separate cages. The experimental protocols were approved by the Animal Research Committee of Tokyo Dental College (Protocol No. 232602).

Micro-CT assessment of bone formation around implants

Micro-CT imaging. After 3 and 8 weeks of healing, animals were sacrificed with an intravascular overdose of 2.5% thiopental sodium (Ravonal, Mitsubishi Tanabe Pharma Corporation, Osaka, Japan) and the femurs were harvested. The specimens were fixed in 10% buffered formalin and underwent micro-CT and 3-dimensional (3-D) stereoscopic imaging (HMX-225 Actis4, Tesco, Tokyo, Japan) and were analyzed with 3-D bone structure measurement software (TRI/3D-BON-BMD-PNTM2, RATOC System Engineering, Tokyo, Japan). Approximately 650 micro-CT slices were scanned with an isotropic resolution of 10 μm within a 6.5 mm range from the coronal top of the implant in the apical direction at an X-ray energy level of 140 kV with a current of 224 μA using a calibration phantom through a 1 mm thick aluminum filter. The calibration phantom consisted of a hydroxyapatite block with seven distinct density layers from 200–800 mg/cm^3 and 1550 mg/cm^3 of aluminum-based stick. Grayscale images were processed using thresholding algorithms based on a given mineral density of the calibration phantom to distinguish titanium and mineralized bone from the background.

Region of interest. The bottom of the inner basic lamellae of the cortical bone at the coronal portion of the implant and the implant surface were set as baseline reference directions for the long and short axes (Figures 2A and B). To evaluate the BV and BMD of the coronal portion of the implants, 3-dimensional bone morphometrical analysis was performed on a region within 1 mm from the baseline of the long axis in the apical direction and within 500 μm from the baseline of the short axis. The short axis was further divided into two regions: from the surface to 100 μm (near zone) and from 100–500 μm (far zone). To obtain control values of BMD, a region of interest was also established encompassing 1 mm^3 within the existing cortical bone at least 500 μm away from the implant surface (Figure 2A).

BV and BMD measurements. BMD and BV measurements were determined by structural morphometry of the 3-dimensional images. BV in the near and far zones around the implants was measured as the percentage bone occupancy in the region of interest. In addition, a bone formation profile was described by plotting BV along the implant long axis within the

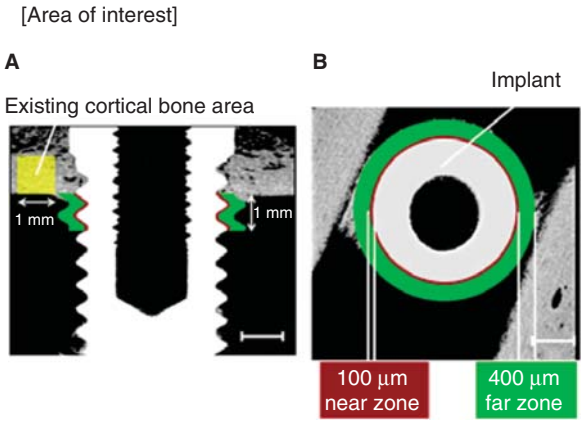

Figure 2. Schematic diagram of the regions of interest. (A) A 1 mm range from the baseline of the long axis in the apical direction and a 1 mm^3 region in the existing cortical bone at least 500 µm away from the implant surface. (B) A 500 µm range from the baseline of the short axis with two regions: from the surface to 100 µm (near zone) and from 100–500 µm (far zone) in longitudinal and cross-sectional grayscale images. Bar is 1 mm.

region of interest. BMDs in the near and far zones around the implants and existing cortical bone were determined within the region of interest using the given mineral densities from the calibration phantom-based standard curve to convert attenuation units to BMD values.

Histological sample preparation. After the micro-CT scanning, specimens were dehydrated in an ascending series of alcohol rinses and embedded in polyester resin (Rigolac 2004; Showa Highpolymer Co. Ltd, Tokyo, Japan) without decalcification. Embedded specimens were cut perpendicular to the short axis of the cylindrical implants at a centerline and ground to a thickness of 100 µm with a cutting and grinding system (Maruto Instrument Co. Ltd, Tokyo, Japan). Two sections per specimen were prepared. Each section had a thickness of ~30 µm and was stained with Villanueva-Goldner stain and observed by light microscopy.

Statistical analysis

Each group contained five samples ($n = 5$). Mann-Whitney U-tests were performed using statistical software (SPSS, Standard Version, SPSS Japan, Tokyo, Japan) to determine differences in BV values in the near and far zones and the BV values at 100 µm intervals within a 1000 µm range from the coronal top of the implant in the apical direction between the non-irradiated and UVC pre-irradiated implant groups. One-way analysis of variance with Bonferroni *post-hoc* tests was performed to determine the differences in BMD between the existing cortical bone, the non-irradiated and the UVC pre-irradiated implants. Statistical significance was set at $p < 0.05$.

Results

Histological observations

Representative histological sections, vertically segmented at the implant center at 3 weeks after implantation, demonstrated relatively thick bone tissue around UVC pre-irradiated implants that had elongated to some extent from the bottom of the inner basic lamellae of the original femur cortical bone along the implant surface (Figure 3B, triangle). In contrast, only small bulging was apparent at the original cortical bone around non-irradiated implants at 3 weeks after implantation (Figure 3A, arrow). Several void spaces (Figure 3C, asterisks) were found at the implant–bone interface on the cortical region of non-irradiated implants, whereas cortical bone tissue attached to the entire surface of UVC pre-irradiated implants (Figure 3D). The mid and apical regions of non-irradiated implants facing the bone marrow allowed cellular attachment to some extent (Figures 3E and G, arrows), but also contained some void spaces (Figure 3G, asterisk) on the surface. In contrast, relatively mature and thick bone tissue with a lamellar structure (Figure 3F, triangles) and dense cellular attachment (Figure 3H, arrowheads) were observed on the mid and apical regions on UVC pre-irradiated implants.

After 8 weeks of implantation, bone tissue continuing from existing cortical bone, along the implant surface, had clearly thickened and developed in the apical direction since the 3-week time point. The bone tissue elongated from the original cortical bone around non-irradiated implants was also relatively developed (Figure 3I, arrow), but appeared to contain less volume than that around UVC pre-irradiated implants at 8 weeks (Figure 3I, triangle). Void spaces remained at the implant–bone interface of the cortical region with non-irradiated implants even at 8 weeks (Figure 3K, asterisks), whereas complete coverage of bone tissue over the cortical region was found for UVC pre-irradiated implant surfaces (Figure 3L). Non-irradiated implant surfaces did show some bone deposition and relatively dense cellular attachment on the mid and apical regions at 8 weeks (Figures 3M and O, arrowheads and triangles). Thick, mature bone tissue with intensive cellular accumulation spread over the mid and apical regions of UVC pre-irradiated implant surfaces (Figures 3N and P, triangles).

Increase of BV around titanium implants after UVC pre-irradiation

Micro-CT-based bone morphometrical analysis revealed that BV in the near zone around implants at 3 weeks after implantation was not significantly different between non-irradiated and UVC pre-irradiated

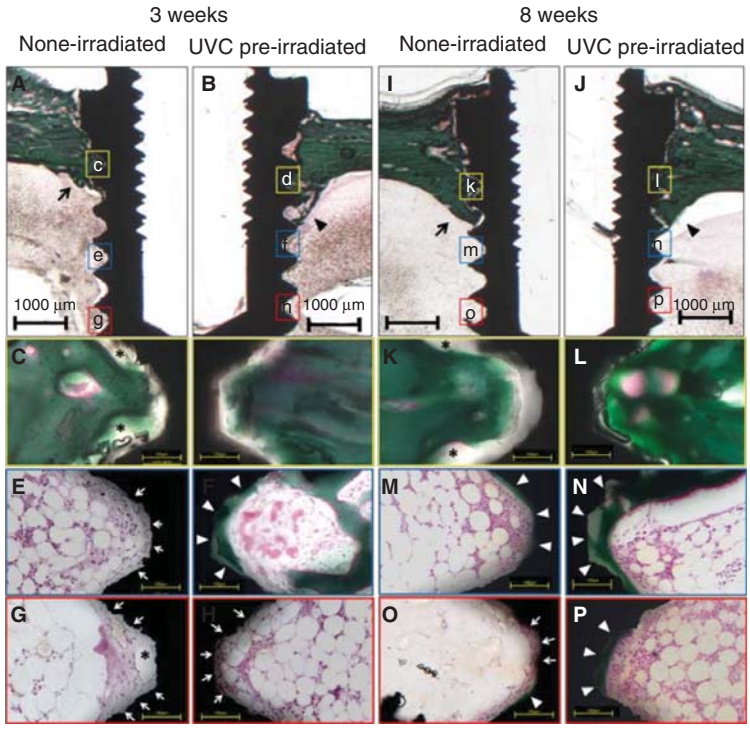

Figure 3. Representative histological images of peri-implant tissue around implants with (B, D, F, H, J, L, N and P) or without (A, C, E, G, I, K, M and O) UVC pre-irradiation at 3 and 8 weeks after placement. Characters in lower magnification images (A, B, I and J) indicates location of the corresponding higher magnification image. Black arrow (A and I) and triangles (B and J); peri-implant bone elongated from the bottom of the inner basic lamellae of the original femur cortical bone along the implant surface. Black asterisks (C, K and G); void spaces at the implant–bone interface of non-irradiated implants. White arrows (E, G, H and O); attached cells on implant surface at the mid or apical regions facing the bone marrow. White triangles; bone deposition on implant surface at the mid or apical regions facing the bone marrow. Bars are 1.0 mm in the lower magnification images (A, B, I and J) and 100 μm in the higher magnification images (C–H and K–P).

implants. However, the value in the far zone was 1.6-times greater around UVC pre-irradiated implants than non-irradiated implants ($p < 0.05$) (Figure 4A). At 8 weeks after implantation, BV in both the near and far zones were significantly different between non-irradiated and UVC pre-irradiated implants. BV values were 1.3-times greater in the near and 1.7-times greater in the far zone around UVC pre-irradiated implants compared with those around non-irradiated implants (Figure 4B).

There were no significant differences in BV at 3 weeks after implantation within a 300 μm distance from baseline of the long axis (Figure 5A), where the BV was ~90–100%, between non-irradiated and UVC pre-irradiated implants. However, BV values around non-irradiated implants at 3 weeks started to decrease from the point of 300 μm from the baseline, reducing to 54, 24 and 8% at 400, 600 and 900 μm from the baseline, respectively. In contrast, the reduction of BV values in the apical direction was gentler around UVC pre-irradiated implants at 3 weeks. The values around UVC pre-irradiated implants at 3 weeks were still ~80% at 400 μm from the baseline, remaining at 46% and 15% at 600 and 900 μm from the baseline. At 3 weeks, the values from 400–900 μm were greater around UVC pre-irradiated implants than around non-irradiated implants ($p < 0.05$). At 8 weeks, despite ~90% BV until 200 μm from the baseline, non-irradiated implants had markedly reduced volume of surrounding bone tissue beyond 300 μm from the baseline. The percentage of bone tissue around non-irradiated implants at 8 weeks was 54 at 500 μm and 20% at 700 μm from the baseline. In contrast, UVC pre-irradiated implants maintained the value of ~90–100% BV until 400 μm from the baseline. The BV values around UVC pre-irradiated implants at 8 weeks remained 60% as far as 700 μm from the baseline. At 8 weeks, the BV from 500–1000 μm was greater around UVC pre-irradiated implants than around non-irradiated implants ($p < 0.05$).

BMD around implants similar to or greater than cortical bone regardless of UVC pre-irradiation

There were consistently no significant differences in mean BMD in the near or far zone between non-irradiated and UVC pre-irradiated implant at 3 or 8 weeks after implantation (Figures 6A and B). At 3 weeks, the BMD value in the existing cortical bone was ~1200 mg/cm^2, which was lower than that in the near zone of UVC pre-irradiated surfaces and comparable to the BMD in the near zone of non-irradiated implants (Figure 6A). At 8 weeks, the BMD value of the existing cortical bone remained at

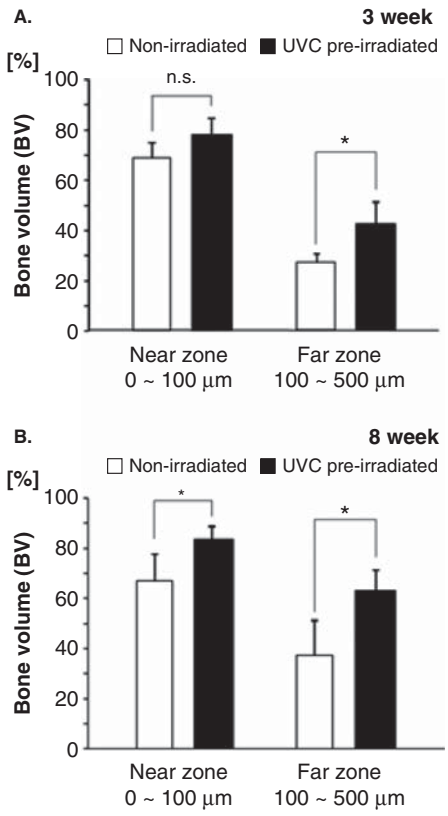

Figure 4. Bone volume (BV) in the near and far zones around UVC pre-irradiated or non-irradiated implants at (A) 3 and (B) 8 weeks after implantation. Data are shown as mean ± SD ($n = 5$). *$p < 0.05$, by Mann-Whitney U-test.

~1200 mg/cm^2, while the BMD values in the near zone of titanium surfaces with or without UVC pre-irradiation and in the far zone of UVC pre-irradiated implants (Figure 6B) were further increased. There was no significant difference in BMD value between the existing cortical bone and the far zone of non-irradiated implants at 8 weeks.

Enhancement of water wettability and reduction of carbon atomic content on implant surface after UVC irradiation

Non-irradiated implants obviously pressed water surface in contact of the apical top (Figure 7A). In contrast, UVC-irradiated implants markedly pulled water. Water swiftly climbed the implant thread and reached the implant platform. The average of static water contact angle on the apical flat surface was 80° on non-irradiated implants, whereas it was 0° on UVC-irradiated implants (Figure 7A) ($p < 0.05$). The carbon peak (285 eV) in the XPS spectrum was strongly detected on non-irradiated implant surfaces (Figure 7B, left spectrum image). These peaks apparently came down after UVC irradiation. The percentage of carbon content was ~40% on the surface before UVC irradiation, which was reduced by UVC to 10% (Figure 7B, right line graph). In contrast, the percentages of titanium and oxygen contents were increased after UVC irradiation. Any apparent change in surface topography was not observed after UVC irradiation (Figure 7C, left contour map). There was no significant difference between non- and UVC-irradiated implants in surface roughness parameters, including Ra and Ry values ($p < 0.05$).

Discussion

The implant site on the femur was standardized as 30 mm in distance from the distal end of the femur of rabbit, which was nearly the diaphyseal region, and consisted of cortical bone and bone marrow tissue without cancellous bone structure. In this model, supporting bone formation around the implant in the cortical region and under the inner basic lamellae can be attributed to bone elongation from the existing cortical bone wall or inner basic lamellae (distant

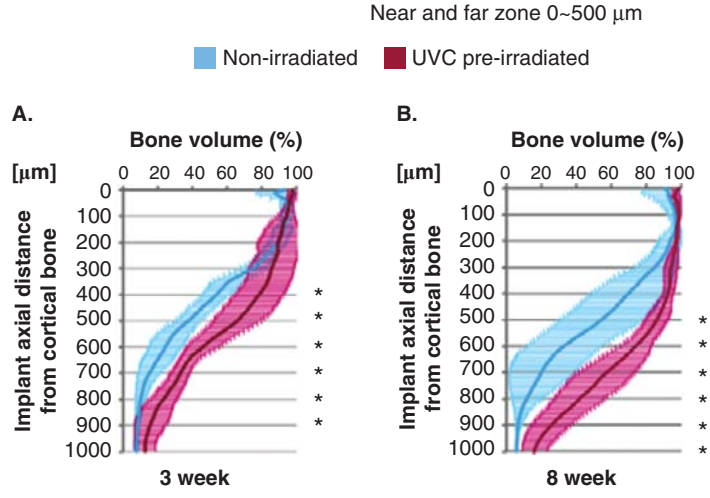

Figure 5. Bone formation profile drawn by plotting BV along the implant long axis within the entire region of interest at (A) 3 and (B) 8 weeks after implantation. Data are shown as mean ± SD ($n = 5$). *$p < 0.05$, Mann-Whitney U-test.

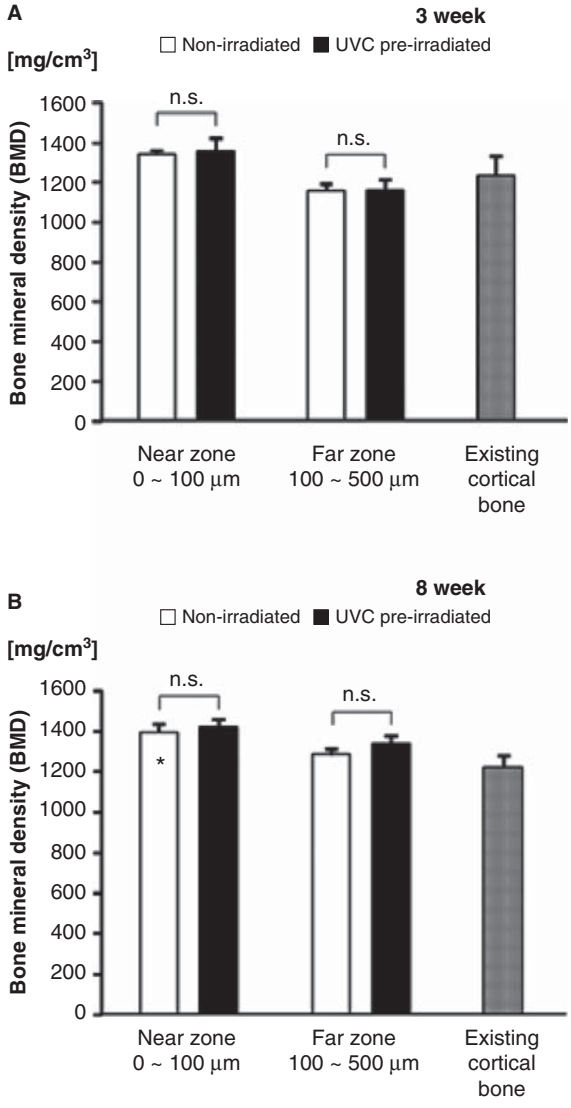

Figure 6. Bone mineral density (BMD) in the near and far zones around UVC pre-irradiated or non-irradiated implants and existing cortical bone at (A) 3 and (B) 8 weeks after implantation. Data are shown as mean ± SD ($n = 5$). Asterisk inside bar indicates significant difference compared with the value in existing cortical bone. $p < 0.05$, Bonferroni multiple comparison.

osteogenesis) and/or direct bone deposition on the implant surface (contact osteogenesis), where osteoblasts in cortical bone and endosteum and osteoprogenitors or mesenchymal stem cells in bone marrow are involved in bone formation. In contrast, bone contact on the implant regions facing only the bone marrow space (the mid and apical regions) can be attributed to purely contact osteogenesis by osteoprogenitor or mesenchymal stem cells in bone marrow. This animal model was able to properly evaluate the supporting bone structure around implants that occurred as a result of the osseointegration capability of the implant surfaces without the confounding effects of original bone structure, except for the cortical bone for initial implant fixation. In addition, the BMD of rabbit femur cortical bone around the implantation site was ~1200 mg/cm^3. This value rivals or surpasses that of human cadaveric mandibular bone (900–1000 mg/cm^3) reported previously using the same system [18] despite small differences in the tomographic condition. In addition, the diaphyseal region of rabbit femur has a flat surface geometry, making it easy to control and standardize the depth of implant placement, and enough cortical thickness to allow initial implant fixation. Therefore, the rabbit femur model used in this study could be considered one of several appropriate experimental models for evaluation of osseointegration capability of screw implants.

The histological observations in this study revealed that UVC pre-irradiated implants allowed cortical bone attachment over the entire surface of the cortical region. Progressive bone formation and cellular accumulation at the mid and apical regions were seen with pre-irradiation, but void spaces at the cortical region and sparse bone deposition on the mid and apical regions were seen on non-irradiated implant surfaces at both 3 and 8 weeks. UVC pre-irradiated implants increased BV along the apical direction of the implant long axis under the inner basic lamellae. Previous *in vitro* studies have demonstrated that UVC pre-irradiation of titanium enhances extracellular adhesive protein deposition, osteoblastic migration and osteoblastic attachment and adhesion, regardless of the type of surface topography [19–23]. Moreover, UVC pre-irradiated titanium surfaces also enhance the function of periosteal cells and activated their interactions with bone marrow-derived osteoblastic cells, which was shown as an increase of individual cellular attachment and proliferation and enhancement of alkaline phosphatase activity and extracellular matrix mineralization under the presence of cellular signals from bone marrow-derived osteoblastic cells [11]. In light of these cellular biological phenomena on UVC pre-irradiated surfaces, UVC pre-treatment may promote contact osteogenesis by enhancing recruitment and attachment of osteogenic cells from cortical bone, endosteum and bone marrow, as well as by activation of interaction between those cells.

In this study, UVC pre-irradiated implants consistently increased the volume of supporting bone within 1 mm from the inner basic lamellae of cortical bone in both the near and far zones as compared with that on non-irradiated implants over 8 weeks of observation, except for the near zone at 3 weeks post-operatively. The bone formation profile from BV data was greater around UVC-irradiated implants than non-irradiated implants in three-fifths of the apical region at both 3 and 8 weeks post-operatively. Histological findings supported the increased BV around UVC pre-irradiated implants determined by bone morphometrical analysis. In addition, there was no significant difference in BMD between both implants over the

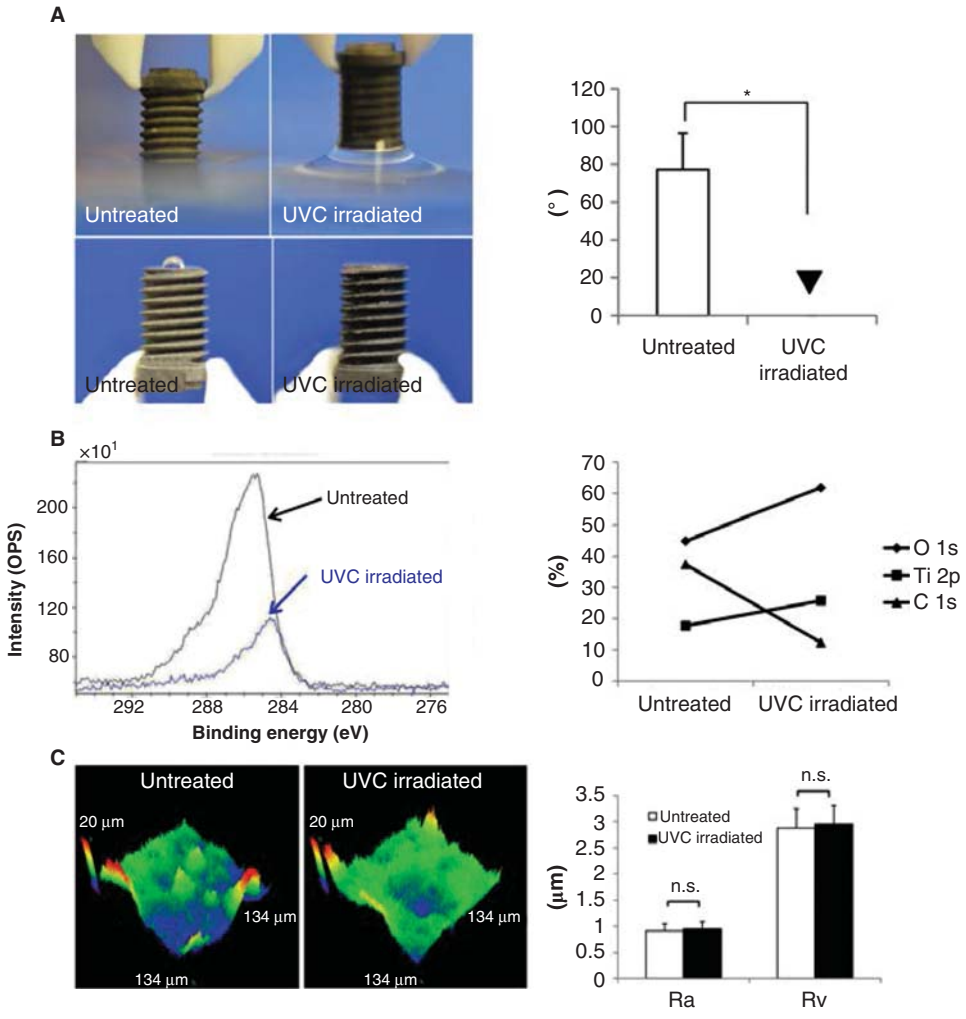

Figure 7. Results of (A) surface wettability, (B) chemical composition and (C) surface roughness of UVC pre-irradiated or non-irradiated implants. Note that UVC-irradiated implants demonstrated a zero-degree water contact angle (arrowhead). Data in repeated measurements are shown as mean ± SD ($n = 5$). Asterisk inside bar indicates a significant difference compared with the value. $p < 0.05$, Mann-Whitney U-test.

observation period of 8 weeks, the magnitude of which rivaled or surpassed that of the existing cortical bone. These results indicate that UVC pre-irradiation increased not only bone–implant contact, but also the formation of cortical-like supporting bone volume without deterioration of bone mineralization.

There was no significant difference in BMD between the implants over the observation period of 8 weeks in this study. BMD values of both UVC pre-irradiated and non-irradiated implants at 8 weeks after implant placement were in the range of ~1300–1400 mg/cm^3 both in the near and far zones, which was similar or greater than the BMD in existing cortical bone at the diaphyseal region of the femur. In addition, mineralized structures around both implants in micro-CT images looked similar to the structure of existing cortical bone. These data indicate that UVC pre-irradiation to titanium implants not only increased the volume of supporting bone formed, but also yielded substantial bone mineral density, similar to that of existing cortical bone. Increases in BV and degree of mineralization are correlated with activation of osteoblastic proliferation and differentiation, respectively [24]. Activation of cellular proliferation often results in delay of cellular differentiation because of the inverse relationship between proliferative activity and progress of cellular differentiation that is typically seen in biology [25,26]. A previous article demonstrated that osteoblastic differentiation was not reduced on UVC pre-irradiated titanium surfaces despite activation of cellular proliferation [9]. Therefore, increases in BV without deterioration of BMD around UVC pre-irradiated implants might result from simultaneous promotion of osteoblastic proliferation and differentiation on the surface.

Many culture studies had demonstrated the underlying biological mechanism on enhancement of osseointegration capability by UVC irradiation as upgraded protein adsorption, osteoblastic adhesion and cellular proliferation without deterioration of osteoblastic cellular differentiation on the surface [9–11,19,20,22,27–29]. As seen in Figure 7, UVC irradiation changed physicochemical properties, but not surface topography on acid-etched implants; this

was characterized by acquirement of superhydrophilicity and reduction of carbon atom on the surface without any change of surface topography. Previous reports also observed these phenomena after UVC irradiation on titanium surface and demonstrated an association with the biological mechanism underlying the upgraded osseointegration capability [9–11,19–21,23,27,29]. Acquirement of superhydrophilicity is recently considered as a factor to enhance osseointegration on implant surface. However, the actual contribution to osseointegration remained to be clarified and is still a subject of controversy [30,31]. Recent culture study indicated that enhancement of wettability alone did not affect osetoblastic attachment on titanium surface [29]. It was known that reduction of hydrocarbon on titanium surface affects wettability on titanium surface. Hydrocarbon is a famous hydrophobic molecule [32]. Ti and O atomic portions on the superficial titanium oxide layer are exposed after removing hydrocarbon, where electrostatic polarity occurred [33]. Therefore, exposed titanium oxide surface inherently reacts with water molecule, a polar molecule, in the aqueous solution or the atmosphere and forms terminal and bridge hydroxyl groups (OH) [34]. Hydroxyl groups contribute to the promotion of hydrogen bond or increase of Van der Waals force and, accordingly, enhancement of surface wettability. Electric charge on the surface of substrate affects osteoblastic cellular attachment [35] and, therefore, osseointegration capability. A previous experiment about UVC-irradiated titanium suggested the possible association between enhanced osteoblastic cellular attachment and change in electrical charge on titanium surface after UVC-irradiation [22]. Change of physical property along with reduction of hydrocarbon might contribute to enhancement of osseointegration capability by UVC irradiation.

Previous clinical studies about implant stability quotient (ISQ) using resonance frequency analysis demonstrated that speed reaching to clinical implant stability during the osseointegration phase was substantially increased on UVC-mediated (photofunctionalized) implants in compromised cases with simultaneous alveolar bone augmentation [36] to or low quality bone tissue with immediate loading [37]. This *in vivo* study supported these clinical outcomes about UVC-mediated activation of the titanium implant surface. Moreover, overload onto implant integrated with bone tissue generally concentrates stress on peri-implant tissue at the implant neck region [3,4], with an increase of risk to cause peri-implant bone resorption and, eventually, implant failure. It is known that peri-implant bone resorption at implant neck region has a risk to cause further increase of stress distribution and subsequent bone resorption at the region [6,7]. Increases of volume of supporting bone tissue around implant beneath inner basic lamellae observed in this study might lead to reduction and deconcentration of stress distribution in peri-implant bone tissue. UVC pre-irradiation might not only enhance establishment of osseointegration but also upgrade the longevity of titanium implant. Further investigation about structural dynamic analysis on supporting bone tissue around the implant should be needed to demonstrate the perspective.

Acknowledgment

This research was supported by Oral Health Science Center Grant hrc8 from Tokyo Dental College, and by a Project for Private Universities: matching fund subsidy from MEXT (Ministry of Education, Culture, Sports, Science and Technology) of Japan, 2010–2012.

Declaration of interest: The authors report no conflicts of interest. The authors alone are responsible for the content and writing of the paper.

References

[1] Sennerby L, Ericson LE, Thomsen P, Lekholm U, Astrand P. Structure of the bone-titanium interface in retrieved clinical oral implants. Clin Oral Implants Res 1991;2:103–11.
[2] Sennerby L, Thomsen P, Ericson LE. Ultrastructure of the bone-titanium interface in rabbits. J Mater Sci Mater Med 1992;3:262–71.
[3] Natali AN, Pavan PG, Ruggero AL. Analysis of bone-implant interaction phenomena by using a numerical approach. Clin Oral Implants Res 2006;17:67–74.
[4] Demenko V, Linetskiy I, Nesvit K, Shevchenko A. Ultimate masticatory force as a criterion in implant selection. J Dent Res 2011;90:1211–15.
[5] Rieger MR, Mayberry M, Brose MO. Finite element analysis of six endosseous implants. J Prosthet Dent 1990;63:671–6.
[6] Kitamura E, Stegaroiu R, Nomura S, Miyakawa O. Biomechanical aspects of marginal bone resorption around osseointegrated implants: considerations based on a three-dimensional finite element analysis. Clin Oral Implants Res 2004;15:401–12.
[7] Yoon KH, Kim SG, Lee JH, Suh SW. 3D finite element analysis of changes in stress levels and distributions for an osseointegrated implant after vertical bone loss. Implant Dent 2011;20:354–9.
[8] Kitagawa T, Tanimoto Y, Nemoto K, Aida M. Influence of cortical bone quality on stress distribution in bone around dental implant. Dent Mater J 2005;24:219–24.
[9] Aita H, Hori N, Takeuchi M, Suzuki T, Yamada M, Anpo M, et al. The effect of ultraviolet functionalization of titanium on integration with bone. Biomaterials 2009;30:1015–25.
[10] Ueno T, Yamada M, Hori N, Suzuki T, Ogawa T. Effect of ultraviolet photoactivation of titanium on osseointegration in a rat model. Int J Oral Maxillofac Implants 2010;25:287–94.
[11] Ueno T, Yamada M, Suzuki T, Minamikawa H, Sato N, Hori N, et al. Enhancement of bone-titanium integration profile with UV-photofunctionalized titanium in a gap healing model. Biomaterials 2010;31:1546–57.
[12] Pearce AI, Richards RG, Milz S, Schneider E, Pearce SG. Animal models for implant biomaterial research in bone: a review. Eur Cells Mater 2007;13:1–10.

[13] NIH consensus development panel on osteoporosis prevention, diagnosis, and therapy. JAMA 2001;285:785–95.
[14] Carter DR, Hayes WC. Bone compressive strength: the influence of density and strain rate. Science 1976;194: 1174–6.
[15] Ikeda S, Tsurukami H, Ito M, Sakai A, Sakata T, Nishida S, et al. Effect of trabecular bone contour on ultimate strength of lumbar vertebra after bilateral ovariectomy in rats. Bone 2001; 28:625–33.
[16] Katsumata T, Nakamura T, Ohnishi H, Sakurama T. Intermittent cyclical etidronate treatment maintains the mass, structure and the mechanical property of bone in ovariectomized rats. J Bone Miner Res 1995;10:921–31.
[17] Butz F, Ogawa T, Chang TL, Nishimura I. Three-dimensional bone-implant integration profiling using micro-computed tomography. Int J Oral Maxillofac Implants 2006;21: 687–95.
[18] Morioka T, Matsunaga S, Yoshinari M, Ide Y, Nakano T, Sekine H, et al. Alignment of biological apatite crystallites at first molar in human mandible cortical bone. Cranio 2012;30: 32–40.
[19] Aita H, Att W, Ueno T, Yamada M, Hori N, Iwasa F, et al. Ultraviolet light-mediated photofunctionalization of titanium to promote human mesenchymal stem cell migration, attachment, proliferation and differentiation. Acta Biomater 2009;5: 3247–57.
[20] Att W, Hori N, Iwasa F, Yamada M, Ueno T, Ogawa T. The effect of UV-photofunctionalization on the time-related bioactivity of titanium and chromium-cobalt alloys. Biomaterials 2009;30:4268–76.
[21] Hori N, Ueno T, Suzuki T, Yamada M, Att W, Okada S, et al. Ultraviolet light treatment for the restoration of age-related degradation of titanium bioactivity. Int J Oral Maxillofac Implants 2010;25:49–62.
[22] Iwasa F, Hori N, Ueno T, Minamikawa H, Yamada M, Ogawa T. Enhancement of osteoblast adhesion to UV-photofunctionalized titanium via an electrostatic mechanism. Biomaterials 2010;31:2717–27.
[23] Miyauchi T, Yamada M, Yamamoto A, Iwasa F, Suzawa T, Kamijo R, et al. The enhanced characteristics of osteoblast adhesion to photofunctionalized nanoscale TiO2 layers on biomaterials surfaces. Biomaterials 2010; 31:3827–39.
[24] Butz F, Aita H, Wang CJ, Ogawa T. Harder and stiffer bone osseointegrated to roughened titanium. J Dent Res 2006;85: 560–5.
[25] Malaval L, Liu F, Roche P, Aubin JE. Kinetics of osteoprogenitor proliferation and osteoblast differentiation in vitro. J Cell Biochem 1999;74:616–27.
[26] Stein GS, Lian JB, Owen TA. Relationship of cell growth to the regulation of tissue-specific gene expression during osteoblast differentiation. FASEB J 1990;4:3111–23.
[27] Yamada M, Miyauchi T, Yamamoto A, Iwasa F, Takeuchi M, Anpo M, et al. Enhancement of adhesion strength and cellular stiffness of osteoblasts on mirror-polished titanium surface by UV-photofunctionalization. Acta Biomater 2010;6:4578–88.
[28] Ohtsu N, Masahashi N, Mizukoshi Y, Wagatsuma K. Hydrocarbon decomposition on a hydrophilic TiO2 surface by UV irradiation: spectral and quantitative analysis using in-situ XPS technique. Langmuir 2009;25:11586–91.
[29] Uchiyama H, Yamada M, Ishizaki K, Sakurai K. Specific ultraviolet-C irradiation energy for functionalization of titanium surface to increase osteoblastic cellular attachment. J Biomater Appl 2014;28:1419–29.
[30] Petzold C, Monjo M, Rubert M, Reinholt FP, Gomez-Florit M, Ramis JM, et al. Effect of proline-rich synthetic peptide-coated titanium implants on bone healing in a rabbit model. Int J Oral Maxillofac Implants 2013;28:e547–55.
[31] Sawase T, Jimbo R, Wennerberg A, Suketa N, Tanaka Y, Atsuta M. A novel characteristic of porous titanium oxide implants. Clin Oral Implants Res 2007;18:680–5.
[32] Taborelli M, Jobin M, Francois P, Vaudaux P, Tonetti M, Szmukler-Moncler S, et al. Influence of surface treatments developed for oral implants on the physical and biological properties of titanium. (I) Surface characterization. Clin Oral Implants Res 1997;8:208–16.
[33] Hanawa T. A comprehensive review of techniques for biofunctionalization of titanium. J Periodontal Implant Sci 2011; 41:263–72.
[34] Henderson MA, White JM, Uetsuka H, Onishi H. Photochemical charge transfer and trapping at the interface between an organic adlayer and an oxide semiconductor. J Am Chem Soc 2003;125:14974–5.
[35] Schneider GB, English A, Abraham M, Zaharias R, Stanford C, Keller J. The effect of hydrogel charge density on cell attachment. Biomaterials 2004;25:3023–8.
[36] Funato A, Ogawa T. Photofunctionalized dental implants: a case series in compromised bone. Int J Oral Maxillofac Implants 2013;28:1589–601.
[37] Suzuki S, Kobayashi H, Ogawa T. Implant stability change and osseointegration speed of immediately loaded photofunctionalized implants. Implant Dent 2013;22:481–90.